Development 140, 2985-2996 (2013) doi:10.1242/dev.092387


# Tubulogenesis in a simple cell cord requires the formation of bi-apical cells through two discrete Par domains

**Elsa Denker[1], Ivana Bočina[2] and Di Jiang[1,*]**

## SUMMARY

Apico-basal polarization is a crucial step in the *de novo* formation of biological tubes. In *Ciona* notochord, tubulogenesis occurs in a single file of cells in the absence of cell proliferation. This configuration presents a unique challenge for the formation of a continuous lumen. Here, we show that this geometric configuration is associated with a novel polarization strategy: the generation of bipolar epithelial cells possessing two apical/luminal domains instead of one, as in the conventional epithelium. At the molecular level, cells establish two discrete Par3/Par6/aPKC patches, and form two sets of tight junctions, in opposite points of the cells. The key molecule controlling the formation of both domains is Par3. Changing the position of the cells within the organ fundamentally changes their polarity and the number of apical domains they develop. These results reveal a new mechanism for tubulogenesis from the simplest cell arrangement, which occurs in other developmental contexts, including vertebrate vascular anastomosis.

**KEY WORDS: Apico-basal polarity, Tubulogenesis, Bipolarity, Par3**

## INTRODUCTION

Tubular organs are important biological systems, as they perform key transport and exchange functions within an organism (Lubarsky and Krasnow, 2003). Biological tube formation is an interesting and challenging morphogenetic process for developmental biologists because it encompasses many changes in cell state and behavior, including cell shape change, cell proliferation, mesenchyme-to-epithelium transition (MET), cell polarization, cell migration and differentiation (Baer et al., 2009; Bryant and Mostov, 2008). The crucial steps of tubulogenesis include the apico-basal (A-B) polarization of the cells that determines where the lumen will form, the secretion of lumen, and the cell and tissue reorganizations that lead to the generation of a continuous luminal compartment. Various strategies for lumen formation and connection exist, among them the formation of a small extracellular lumen that expands in the center of tissue (chord hollowing) or individual cells (cell hollowing), the wrapping of a sheet of cells around a lumen, and the clearing of internal cells through apoptosis (cavitation) (Baer et al., 2009; Bryant and Mostov, 2008). Most of these processes are initiated by the specific differentiation of a single apical domain in each individual cell within the tissue. At the molecular level, this specification involves the highly conserved Par complex (Par3, Par6, aPKC), whereas the basolateral domain is associated with the Scribble/Lgl/Dlg complex (McCaffrey and Macara, 2009; Suzuki and Ohno, 2006). The apical domain and basolateral domain are separated by apical/lateral junctions that seal the epithelial tissue.

In MDCK cells, the best-studied model system for tubulogenesis, cells are initially organized in a cluster with at least two cells present in a cross-section. During the initial steps of tube formation, MDCK cells undergo MET, through which the inner surface of individual cells in the cluster differentiates into an apical domain, where lumen secretion takes place. Each cell thus possesses a single and simple A-B polarity axis, with the basal end maintaining a continuous contact with the surrounding matrix. The *de novo* formed apical domain then expands and aligns with the apical domains of neighboring cells, ensuring the formation of an unobstructed lumen. In contrast to the *in vitro* MDCK model, many biological tubes in animal development form from cells in a simpler configuration: a cord of cells arranged in a single file. These include capillary vessels and the *Drosophila* trachea. In this configuration, a new challenge appears for generating a continuous tube: connecting luminal compartments emerging between the consecutive cells, without altering the integrity of the structure and causing the lumen to enter into contact with other compartments. In *Drosophila* trachea, the problem is solved by a fusion/fission event between the two membrane domains of the cell that are in contact with the two separate lumen pockets, creating a central hole that allows the two lumen pockets to merge (Samakovlis et al., 1996). We recently developed a new model for *in vivo* studies of tubulogenesis, the notochord of *Ciona intestinalis*, which provides a simple system to explore this process. *Ciona* notochord is composed of 40 large and geometrically identical cells that no longer divide, so that tubulogenesis involves only the remodeling of cell shape and tissue configuration (Denker and Jiang, 2012; Dong et al., 2009; Jiang and Smith, 2007). During development, notochord cells are also initially aligned in a single file. Tubulogenesis begins with the *de novo* formation of central and extracellular lumen pockets between adjacent cylindrically shaped cells. Lumen connection does not involve membrane fission and fusion, but is accomplished through shape change of individual cells, leading to an overall tissue reorganization (Dong et al., 2009; Jiang and Smith, 2007). Each cell undergoes a bidirectional crawling movement that leads to the retraction of the diametrically opposite cell tips and drives a reverse intercalation process (Dong et al., 2009). Recently, an almost identical tubulogenesis mechanism has been described during the anastomosis of zebrafish intersomitic vessels (Herwig et al., 2011), confirming the potential relevance of the notochord system.

Intriguingly, the formation of extracellular luminal compartments at both ends of individual cells must imply that two distinct domains

[1]Sars International Centre for Marine Molecular Biology, University of Bergen, Thormøhlensgt. 55, N-5008 Bergen, Norway. [2]Department of Biology, Faculty of Natural Sciences, University of Split, Teslina 12, 21000 Split, Croatia.

*Author for correspondence (di.jiang@sars.uib.no)

**Accepted 1 May 2013**

of the cells have to adopt an apical identity. To explore this hypothesis, we performed an in-depth molecular and subcellular study of the polarity mechanisms underlying the very first steps of notochord tubulogenesis.

## MATERIALS AND METHODS

### Animals and embryos

*Ciona intestinalis* were collected in Bergen, Norway, or purchased from Roscoff Marine Station, France. Eggs were extracted and mixed in seawater with sperm from other individuals. After fertilization, the embryos were dechorionated and cultured at 13°C or 16°C.

### Plasmids

Full-length *par3*, *par6*, *apkc*, *scribble* and *dlg* were amplified from clones in the *Ciona intestinalis* gateway-compatible cDNA library prepared by Mike Gilchrist (NIMR, London, UK), and cloned into the pCR8/GW/TOPO (Invitrogen) to obtain entry clones. These entry clones were recombined using the Gateway LR reaction (Invitrogen) into previously described destination vectors (Dong et al., 2009) to obtain N- or C-terminal turboGFP or mCherry fusion constructs (see supplementary material Table S1 for more details). *Lgl* and *zo1* entry clones from François Robin (University of Chicago, IL, USA), and rat *myr-apkc* plasmid from Brad Davidson (University of Arizona, Tucson, AZ, USA) were used to generate C-terminal fusion constructs. Lifeact-mEGFP, E-Cadherin-mCherry and Slc26aα (SLC26-2)-mCherry have been described previously (Dong et al., 2009). Stratagene Quick Change II Mutagenesis Kit was used to generate aPKC K197W, Par3 S732A and Par6 ΔaPKC-BD (see supplementary material Table S1 for more details).

### Electroporation and morpholino injection

Electroporation was performed as described previously (Dong et al., 2009). Par3 translation-blocking morpholino (CCAAAACACACGGTAACT-TTCATTC) was designed based on French, Japanese and Norwegian sequences. The FITC-coupled control morpholino (CCGGAATATGTA-CATTCGTGGTCAA) contained a comparable GC content. Morpholino was injected with Alexa488-coupled dextran (D22910, Invitrogen) following previously published protocols (Christiaen et al., 2009).

### *In situ* hybridization

*par3*, *scribble*, *dlg* and *cdc42* clones from the *Ciona intestinalis* release 1 gene collection (clone numbers in supplementary material Table S1) were used to prepare antisense probes using *Not*I and T7 RNA polymerase, and sense probes using *Xho*I and Sp6 RNA polymerase. For other genes, probes were prepared from the entry clones described above, using *Nco*I (*lgl*), *Xho*I (*par6*) or *Pst*I (*zo1*), and T7 RNA polymerase. Digoxygenin-coupled probes were synthesized using Roche DIG RNA Labeling Kit following manufacturer's instruction. *dlg*, *par6*, *lgl* and *zo1* probes were fragmented to 100-200 bp through alkaline hydrolyzation. *In situ* hybridization was carried out following a published protocol (Wada et al., 1995), except the acetylation step was omitted.

### Antibody staining

Rabbit anti-rat PKCζ (Santa Cruz SC-216; 1/200), rabbit anti-*Drosophila* Bazooka/Par3 (Wodarz et al., 1999) (1/200) and mouse anti-Slc26aα (Dong et al., 2009) (1/1000) were used with secondary antibodies anti-rabbit Alexa 568 and anti-mouse Alexa 488 (Invitrogen A11011 and A10680; 1/1000) for immunostaining following a published protocol (Dong et al., 2009). The embryos were counterstained with 3 units/ml BODIPY FL phalloidin (Invitrogen) or 1 μg/ml DAPI.

### Laser scanning confocal microscopy

Confocal images were taken with a Leica TCS SP5 confocal laser scanning microscope with 40×oil immersion objective (NA 1.25) at 0.5 to 1 μm intervals. For time-lapse, embryos were mounted in Lab-Tek chamber (ThermoScientific/Nunc). Image analysis and processing were performed with Leica TCS SP5 systems LAS AF software, Adobe Photoshop and ImageJ. Unless otherwise specified, the projections are maximum projections.

### Transmission electron microscopy

Late tailbud stage embryos were fixed with 4% paraformaldehyde and post-fixed in 1% osmium tetroxide. The samples were embedded in Durcupan resin (Fluka). Ultrathin sections (60 nm) were counterstained with uranyl acetate and lead citrate and observed using Jeol JEM 1230 transmission electron microscope.

## RESULTS

To present the results, we follow previous staging of notochord morphogenesis (Dong et al., 2009): stage IV, A-P elongation of the cells and narrowing in diameter; stage V, growth of lumen pockets between notochord cells; stage VI, tilting and connection of the lumen pockets.

To investigate the molecular mechanisms underlying the A-B polarization, we chose a candidate gene strategy. We first checked whether the *Ciona intestinalis* homologues of members of the Par and Scribble complexes were expressed during notochord morphogenesis. *In situ* hybridization showed that *par3*, *par6*, *discs large*/*dlg*, *lethal giant larvae*/*lgl* and *scribble*/*scrib* were strongly expressed in the notochord at stages IV and V, prior to and during lumen formation (supplementary material Fig. S1A-D,I,J). Immunofluorescence showed that Par3 and aPKC proteins were present and displayed a specific subcellular localization in notochord cells at the same stages (supplementary material Fig. S1L-N, with a staining in epidermal cells as control in Fig. S1O-O″). *cdc42*, an integral component of Par complex in many systems, was also expressed in the notochord cells (supplementary material Fig. S1G,H). As these results were compatible with an involvement in cell polarization, we thus adopted a mosaic transient transgenesis method to characterize the protein localization in individual cells *in vivo*. Fluorescent fusion proteins were expressed in the notochord specifically, using the *brachyury* enhancer followed by the *fog* basal promoter (eBra-bpFOG) (Dong et al., 2009).

### Par3, Par6 and aPKC are spatially restricted to two sites where the apical domains appear and the lumen pockets form

At the onset of stage IV, individual notochord cells have a flat cylindrical shape, so that the whole structure resembles a 'stack of coins' along the A-P axis. Each cell is in contact with two other notochord cells (except the first and last cells) and has two discoidal cell-cell interfaces, which represent two separate lateral domains. The rest of the cell surface, which contacts the surrounding extracellular matrix, corresponds to a single and circumferential basal domain. Par3 and Par6 initially presented a faint and broad localization at each of the lateral domains (Fig. 1Aa,b; supplementary material Movie 1). Progressively, the two proteins became enriched at the central region of the domains, with a significant overlap between each other (Fig. 1Ac-c″; supplementary material Movie 1). At this stage, Slc26aα, a specific marker for the luminal domain [SLC26-2 in Dong et al. (Dong et al., 2009)], had no specific distribution (Fig. 1Ad,e,Ea; supplementary material Movie 2). As cells proceeded further with A-P elongation and the narrowing that defines stage IV, Par3 and Par6 became strictly restricted to a discrete area, where aPKC was also enriched, and the three proteins significantly co-localized (Fig. 1Ba-b″; supplementary material Movie 1). The domain occupied about a third of each lateral domain in diameter, as a centered disk. Par6 was slightly more extended towards the basal side than Par3. At the same time, Slc26aα also began to accumulate in the same region (Fig. 1Bc-d,Eb; supplementary material Movie 2). The colocalization of all four proteins, Par3, Par6, aPKC and Slc26aα at

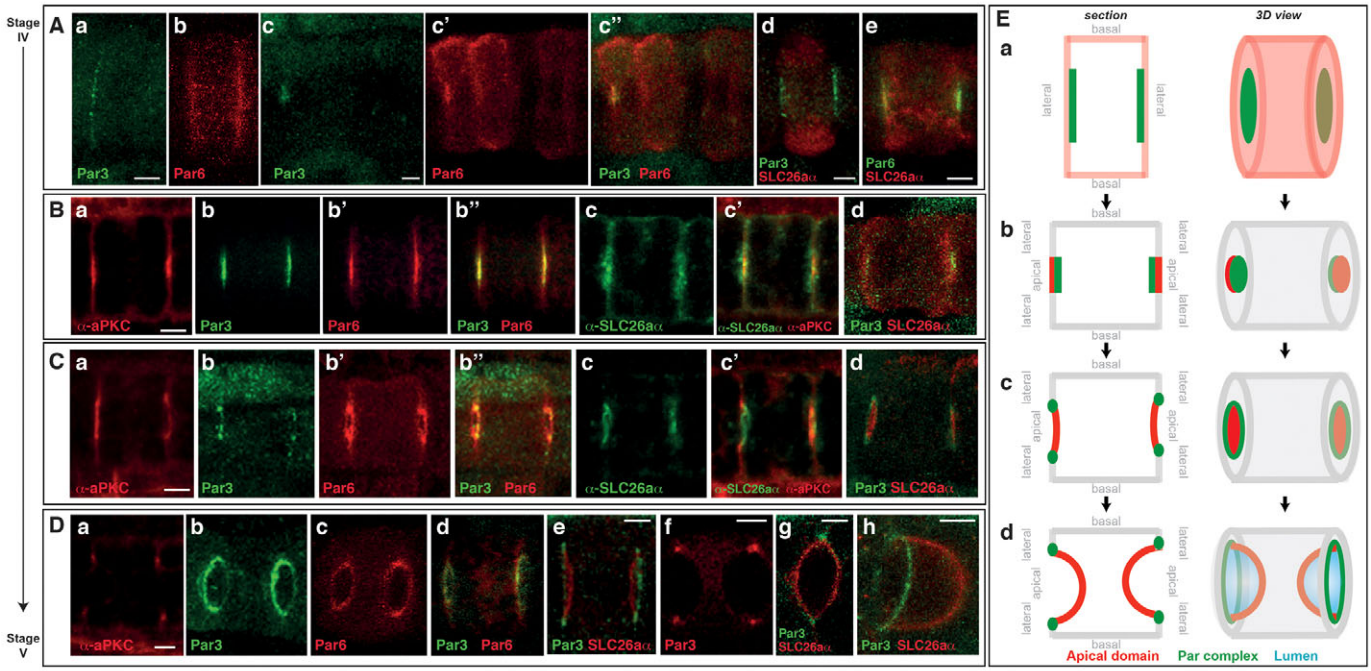


**Fig. 1. Par3, Par6 and aPKC localization correlates with apical domain specification and lumen formation in notochord cells.** (**A-D**) Confocal images of notochord cells expressing fluorescent fusion proteins or antibody-stained. (Ba,Da) Longitudinal sections; all others are projections. (**E**) Interpretative diagrams. (A,Ea) Early stage IV (chronologically: Aa and Ab; Ac-c″; Ad and Ae). (B,Eb) Mid-stage IV; (C,Ec) late stage IV; (D,Ed) early stage V. Scale bars: 5 μm.

the center was, however, transient. Still before the presence of any visible lumen, the disk-shaped Par3, Par6 and aPKC domain progressed into a ring shape, and all three proteins were excluded from the center (Fig. 1Ca-b″; supplementary material Movie 1). By contrast, Slc26aα now strictly filled the inside of the ring, without any colocalization with the Par complex proteins (Fig. 1Cc-d,Ec; supplementary material Movie 2). The disassociation of Par complex from the center clearly indicated the presence of an individualized and functionally differentiated apical domain, which at this point showed almost no concavity, with no detectable open luminal space. Throughout the rest of stage V, the apical, Slc26aα-positive domain expanded in diameter, whereas the lateral domain reduced. At the same time, the Par-positive ring, which located at the apical-lateral junction, accordingly increased in diameter (Fig. 1Da-e; supplementary material Movie 1). The apical domain developed an increasing inward curvature, and the extracellular space was filled with lumen (Fig. 1Df-h,Ed; supplementary material Movie 2). The evolution of these markers on both ends of the notochord cells was identical, and often synchronous.

## Discs large, Scribble and Lethal giant larvae are basolaterally localized

At the beginning of stage IV, Lgl and Dlg were localized at both the basal and lateral domains (Fig. 2Aa,b). At this stage, Par6 overlapped with Lgl on the two lateral sides of each cell (Fig. 2Ac,Ea), whereas Slc26aα was not yet restricted to the central region of the lateral domains (Fig. 2Ad,Ea). As the development proceeded, when Par6 and Par3 accumulated specifically at the prospective apical domains (Fig. 2Ba-c), Dlg began to be excluded from this area (Fig. 2Bd,Eb). Just before lumen formation, the center of the lateral domains was cleared of both Par and Lgl/Dlg, and was filled with Slc26aα (Fig. 2C,Ec). Par3 and Par6 now formed rings at the boundary between the Lgl/Dlg and the Slc26aα-positive domains. Lgl and Dlg clearly did not overlap either with the Par complex or with the apical marker. As lumen expanded, the Lgl/Dlg domain reduced, in parallel with the reduction of the lateral domains, and the expansion of both the apical/Slc26aα domain and Par ring at the apical-lateral junction (Fig. 2Da,a′,Ed). Scrib showed the same basal/lateral pattern, without any detectable colocalization with Par6 at the apical/lateral junctions (Fig. 2Db).

## Apical concentration of Par complex precedes the downregulation of adherens junctions and correlates with the appearance of tight junctions

To detect adherens junctions, we used a *Drosophila* E-Cadherin (E-Cad) fusion construct (Roure et al., 2007). At early stage IV, E-Cad localized at the entire lateral domains (Fig. 3Aa). Later, the protein was excluded from the central region of the lateral domain, which appeared as a wide ring around the apical domain (Fig. 3Ab-d). As lumen expanded, the apical limit of the E-Cad-positive domain was pushed out centrifugally, correlating with the reduction of the lateral domain and the concurrent expansion of the apical domain. A comparison with Lgl showed a constant overlap of the two markers before and during lateral domain reduction (Fig. 3B). A closer analysis, however, revealed that the overlap was not total, with a domain near the apical/lateral junction occupied only by E-Cad (‘1’ in Fig. 3Bc), then an overlap domain (‘2’ in Fig. 3Bc) and finally a domain towards the lateral/basal junction occupied only by Lgl (‘3’ in Fig. 3Bc). Examination of the relative positions and dynamics of adherens junctions and the Par complex showed that central Par3 accumulation preceded central E-Cad downregulation (Fig. 3Ca). Although both proteins coexisted in the central region, they were spatially separated, with Par3 proteins being interior of the E-Cad-labeled membrane. As lumen expanded and E-Cad formed a ring,

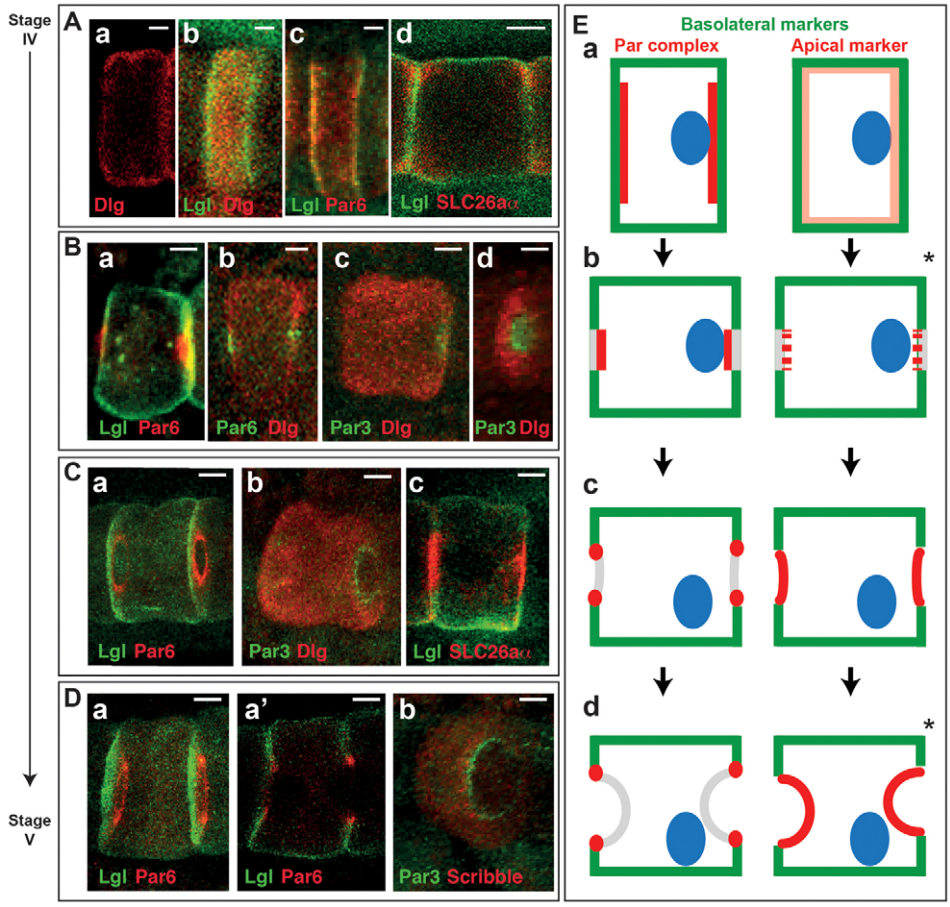


**Fig. 2. Lgl, Dlg and Scribble localize at the basolateral domains.** (**A-D**) Confocal images of notochord cells expressing fluorescent fusion proteins. (Aa,Bb,Cc,Da′) Longitudinal sections; all others are projections (Bd,Ca,Cb,Da,Db are rotated to show the lateral surface). (**E**) Interpretative diagrams. Asterisks indicate conclusions deduced from results in Figs 1 and 2. (A,Ea) Early stage IV; (B,Eb) mid-stage IV; (C,Ec) late stage IV; (D,Ed) early stage V. Scale bars: 5 μm.

the Par3 domain was enclosed in it, as a concentric and non-overlapping ring (Fig. 3Cb). The co-expression of Par6, Slc26aα and E-Cad showed that the Par6 ring sat precisely between the apical domain (Slc26aα disk) and the adherens junction domain (E-Cad ring), with no overlap between these three regions (Fig. 3Cc,d).

Tight junctions were monitored using a *Ciona* ZO1 fluorescent fusion (Sherrard et al., 2010). The expression of *zo1* in the notochord was confirmed by *in situ* hybridization (supplementary material Fig. S1F,K). ZO1-tGFP, which had no discernible localization at the end of intercalation, progressively accumulated at the prospective apical domain at early stage IV (supplementary material Movie 3), before, interestingly, the accumulation of Slc26aα (Fig. 3Da). When Slc26aα began to condense at the apical domain, the ZO1 signal appeared more intense and transformed to a small ring that enclosed the Slc26aα patch (Fig. 3Db; supplementary material Movie 3). As the lumen expanded, the ZO1 domain presented as a progressively larger ring at the apical/lateral border, completely enclosing the Slc26aα-positive apical domain but without any overlap, similar to the Par proteins (Fig. 3Dc-f; supplementary material Movie 3). We further investigated the spatiotemporal dynamics of ZO1 by comparing it with that of E-Cad (Fig. 3E). Early ZO1 accumulation preceded the central E-Cad downregulation, similar to the Par proteins (Fig. 3Ea). However, after this transient configuration, we never found any colocalization of the two markers, confirming ZO1 was not present at the level of adherens junctions and could be used as a specific marker for tight junctions. Later ZO1, but not E-Cad, was found in the prospective apical domain (Fig. 3Eb,b′). As the apical domain formed and enlarged, it was free of both junction proteins but was bordered by a thin ZO1 ring, which was in turn was enclosed by the large E-Cad ring (Fig. 3Ec,c′). This spatial relationship was maintained during apical domain growth and lumen expansion (Fig. 3Ed-g). Transmitted electron microscopy confirmed the presence of typical tight junctions, precisely at the apical/lateral boundary (Fig. 3G), exactly as in vertebrates. The similarity between the Par proteins and ZO1 was strongly in favor of a localization of the Par complex at tight junctions. To confirm this, we co-expressed Par6 or Par3 with ZO1. ZO1 clearly colocalized with Par3/Par6 before lumen formation (Fig. 3Fa; supplementary material Movie 3) and at the lumen formation stage (Fig. 3Fb; supplementary material Movie 3), demonstrating the junctional position of the Par complex (Fig. 3Ec).

## Par3 is necessary for lumen formation

Our observations suggested a strong correlation between the specification of the apical domain, the formation of tight junctions and the subcellular localization of the Par complex. We tested this idea further with a functional approach, through the knockdown of *par3*. Because Par proteins are involved in the polarization of many cell types during early development, a full knockdown approach was unlikely to be possible without disrupting development at early stages. However, the fact that at tailbud stages *par3* was expressed at a much higher level in the notochord (also in the central nervous system) than in other tissues suggested a stronger requirement of Par3 in the notochord at these stages (Fig. 4A; also see supplementary material Fig. S1L,P-S for protein expression). Moreover, even though Par3 has been shown to be asymmetrically distributed in blastomeres of *Phallusia mammillata* embryo (Patalano et al., 2006), it is in the form of a

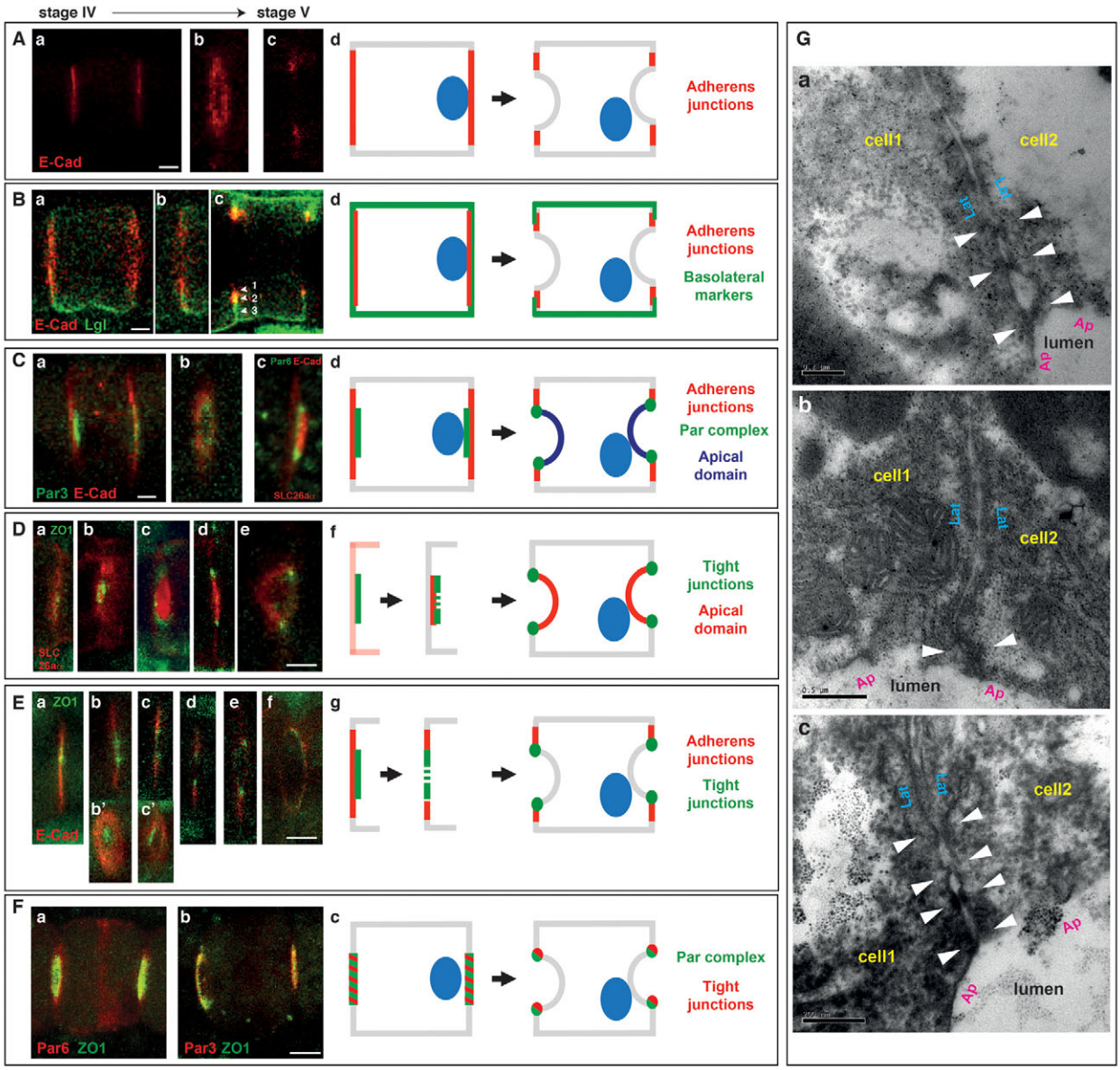


**Fig. 3. Apical domain specification by the Par complex correlates with adherens junction downregulation and tight junction formation.** (**A-F**) Confocal images of notochord cells expressing fluorescent fusion proteins. (Ac,B,Da,Dd,De,Ea-Ee) Longitudinal sections; all others are maximum projections (except Cb, which is a standard deviation projection). (Ab,Cb,Db,Dc,Eb′,Ec′,Ef) Rotated to show the lateral surface. In Bc, '1' is an E-Cad only domain, '2' is an E-Cad and Lgl co-localized domain, and '3' is a Lgl-only domain. (**G**) Transmission electron microscopy images showing the lateral/apical junction at stage V. White arrowheads indicate tight junctions. Ap, apical membrane; Lat, lateral membrane. Scale bars: 5 µm in A-F; 0.2 µm in Ga,Gc; 0.5 µm in Gb.

maternal protein that would not be affected by a morpholino (MO). For similar reasons, a MO-mediated reduction strategy was used successfully to disrupt the late functions of Par3 in the separation of the eye fields and in retinal lamination in zebrafish (Wei et al., 2004).

We injected a translation-blocking MO (supplementary material Fig. S2A) into one-cell stage embryos at a range of concentrations. We confirmed that the Par3 protein level was specifically reduced by comparing the fluorescence of a plasmid-encoded mCherry-tagged Par3 (that can be targeted by the Par3 MO with only two mismatches) with that of a control co-injected plasmid-encoded meGFP-tagged LifeAct (Fig. 4B). The depletion was dose dependent, with a very mild reduction at 0.25 mM of MO (compare Fig. 4Bb and 4Ba), a significant reduction at 0.5 mM (Fig. 4Bc) and a complete reduction at 1 mM (Fig. 4Bd). At 0.1 mM, both the control MO and Par3-MO had no effect on development (Fig. 4Ca,b). When the concentration was raised to 0.25 mM, a very small proportion of the Par3 morphants were slightly shorter compared with the controls (Fig. 4Cc). By contrast, when the MOs were injected at 1 mM, almost all Par3 morphants stopped developing before gastrulation (Fig. 4Ch,i), whereas most control morphants were still normal (Fig. 4Ca). We thus decided to focus on the concentration of 0.5 mM that gave rise to a wide range of phenotypes (Fig. 4Cb-i,D,E). The dose dependence of the phenotype was clearly visible, as the strength of the phenotype correlated with the fluorescence intensity after injection (supplementary material Fig. S2B). We classified the phenotypes into four categories: I to IV. Embryos in category I (only 20%,

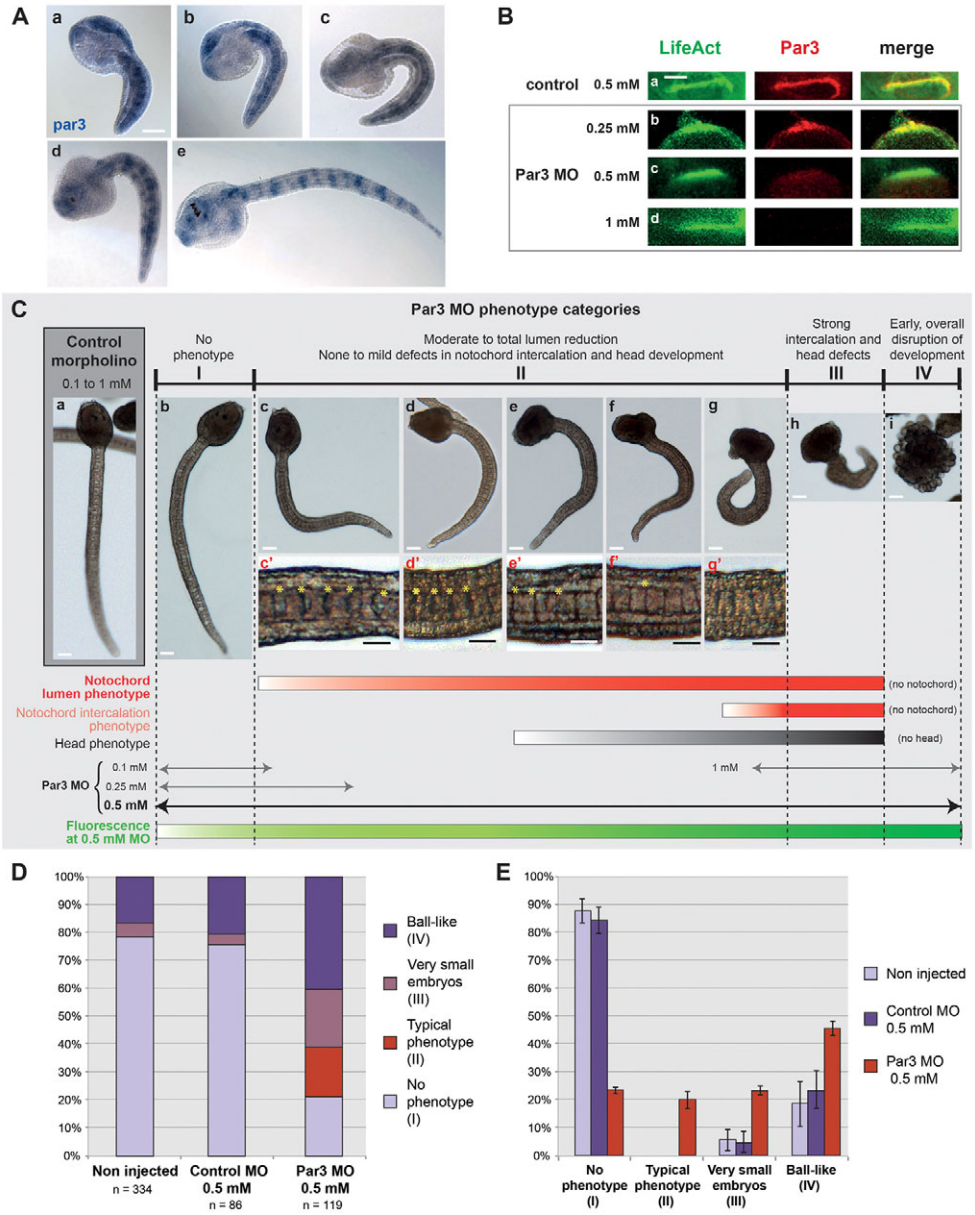


**Fig. 4. Par3 knockdown impairs lumen formation.** (**A**) *par3* expression from mid-tailbud I to late tailbud II in the notochord and various head structures. (**B**) Fluorescence intensity of LifeAct-mEGFP and mCherry-Par3 at the lateral domain in embryos injected with different concentrations of morpholino showing a specific and dose-dependent reduction of Par3 with Par3 MO. (**C**) Dose-dependent range of phenotypes observed with various Par3 MO concentrations (Cb-i) compared with the control MO (Ca). Higher magnifications are shown in Cc′-g′. Asterisks indicate lumen pocket. Phenotype categories are described in the results. (**D**) Average proportions of embryos in different phenotype categories in three treatments: no injection, 0.5 mM control MO and 0.5 mM Par3 MO. (**E**) Percentages of embryos displaying each category of phenotype in the three treatments (mean ± s.d.). Scale bars: 50 μm in A,Ca-i; 20 μm in Cc′-g′; 2 μm in B.

compared with nearly 80% in control) were normal. The second and most interesting category of embryos (category II, 20%, but completely absent from the controls) had developed normally but their tail was shorter (60 to 75% of the control tail length) and the notochord cells, though intercalated correctly and elongated normally, failed to generate lumen pockets (Fig. 4Cc-g′). At this concentration, the protein level was reduced significantly but not completely (Fig. 4Bc). The more severely affected embryos displayed a very reduced tail (shorter than 50% of the normal length), owing to a reduced A-P elongation of the notochord cells and moderate to strong intercalation defects (Fig. 4Ch). As these embryos were also present as a small fraction in the control, they were grouped into a distinct category (category III, around 20% in the Par3 morphants, versus around 5% in the controls). In categories II and III, the severity of the notochord phenotype was also coupled with an increasing defect in head formation, which correlated with the expression of the gene in the head. The category IV corresponded to the embryos that failed to develop before gastrulation (40% in the Par3 morphants versus 20% of the controls), which also represented the majority of the embryos after injection of the Par3 MO at 1 mM. In summary, these results indicate that Par3 is essential for lumen formation, a crucial event in notochord tubulogenesis.

## Par3 is necessary for apical localization of apical markers, tight junction formation and the downregulation of basolateral and adherens junction markers

We performed a molecular analysis of the phenotype by systematically examining the subcellular localization of markers in the category II embryos, which had very reduced or no lumen. In Par3 morphants, the apical marker Slc26aα was widely distributed on all membrane domains, with a slight concentration in the center of the lateral domains, where the apical domains and the lumen pockets would normally emerge (Fig. 5Aa-b″). aPKC, which was specifically restricted at the level of tight junctions in controls, was more broadly distributed on all cell membrane, with a very mild accumulation in the center of the lateral domains. A

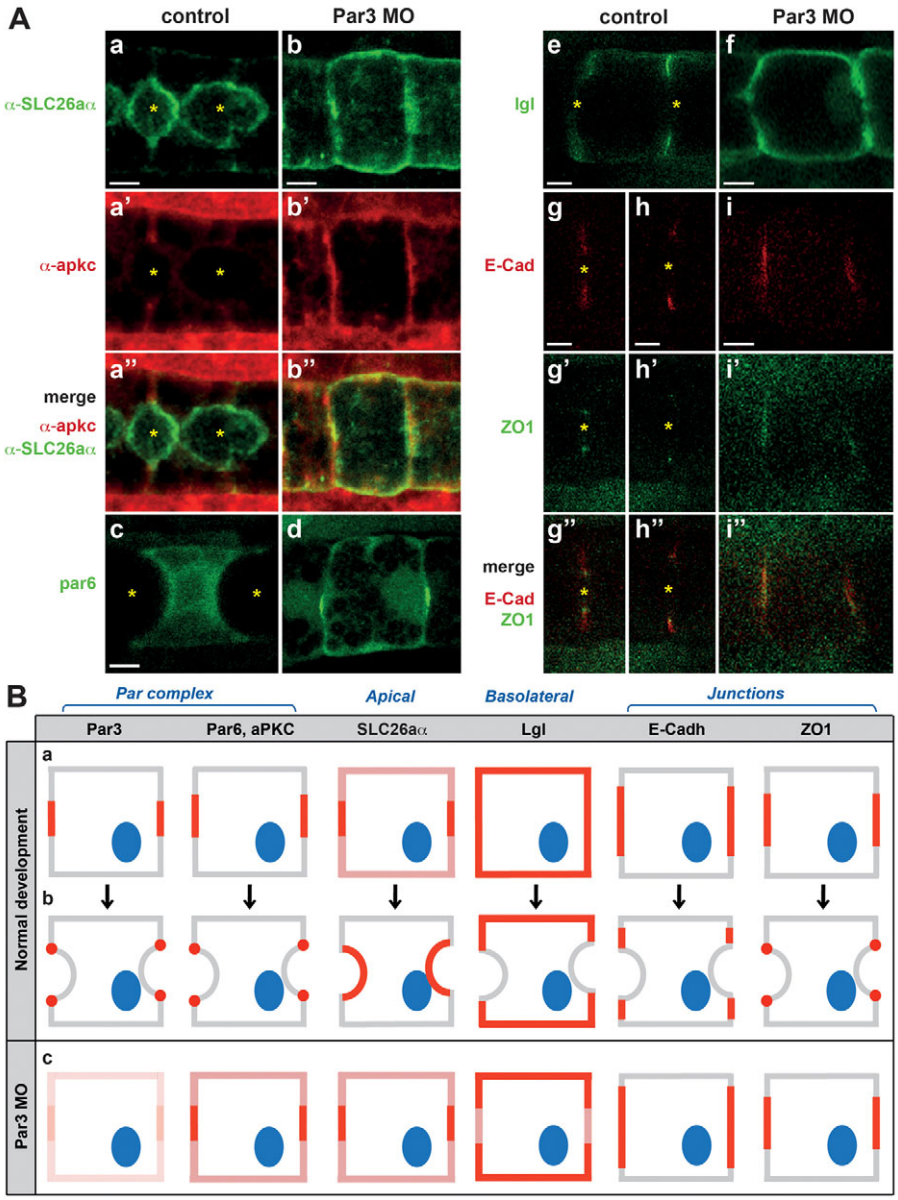


**Fig. 5. Par3 knockdown impairs the A-B cell polarization that is necessary for lumen formation.** (**A**) Confocal images of immunostained (Aa-b″) or live notochord cells expressing fluorescent fusion constructs (Ac-i″) in control and Par3 morphants at stage V. Asterisks indicate lumen pockets. Scale bars: 5 μm. (**B**) Diagrams comparing the localization of markers from stage IV (Ba) to stage V (Bb) during normal development to Par3 morphants at stage V (Bc).

similar pattern was observed for Par 6 (Fig. 5Ac,d). Lgl, which was normally downregulated from the center of the lateral domains (Fig. 5Ae), was retained at this site in the morphants, presenting as an almost continuous localization pattern spanning the entire lateral interface (Fig. 5Af). Similarly, E-cad did not show any central interruption (Fig. 5Ag-i″), while ZO1 showed a central accumulation that did not lead to a segregation of tight junctions around the lumen. These results indicate that the failure to develop the lumen pockets and undergo tubulogenesis was due to a polarization defect in the cells. Though the overall re-localization of the markers had started, probably owing to the residual amount of Par3 protein available, the process could not go further. As a consequence, the cell remained at a stage similar to the earlier stage of normal development, where A-B polarization was just initiated (Fig. 5B). The defect in polarization could not be explained by a general slowdown of the development resulting from MO injection, as control MO did not have this effect, and other anatomical structures in Par3 MO-injected embryo developed normally.

## aPKC mislocalization does not affect tight junction positioning and lumen formation

A complementary approach to study the involvement of the Par complex is to disrupt aPKC localization, which in other models can alter the normal activation pattern of the complex (Macara, 2004). Inhibition of aPKC disrupts cell polarization and lumen formation in MDCK cells (Bryant et al., 2010). We overexpressed myristoylated apkc (myr-apkc) in the notochord cells, and at stage IV this led to a bright and homogenous localization of signal at all membrane domains (supplementary material Fig. S3). Surprisingly, the construct did not affect lumen formation (supplementary material Fig. S3A-B′). When the amount of DNA was raised, the cells failed to intercalate (Fig. 6B,E; supplementary material Fig. S3B,B′), but were still able to form lumen (supplementary material Fig. S3B,B′). More intriguingly, tight junctions were strictly positioned at the forming apical domain in notochord without (supplementary material Fig. S3C) and with impaired intercalation (Fig. 6E), and then at the apical-lateral junction (supplementary material Fig. S3D), identical to the control. A detailed examination

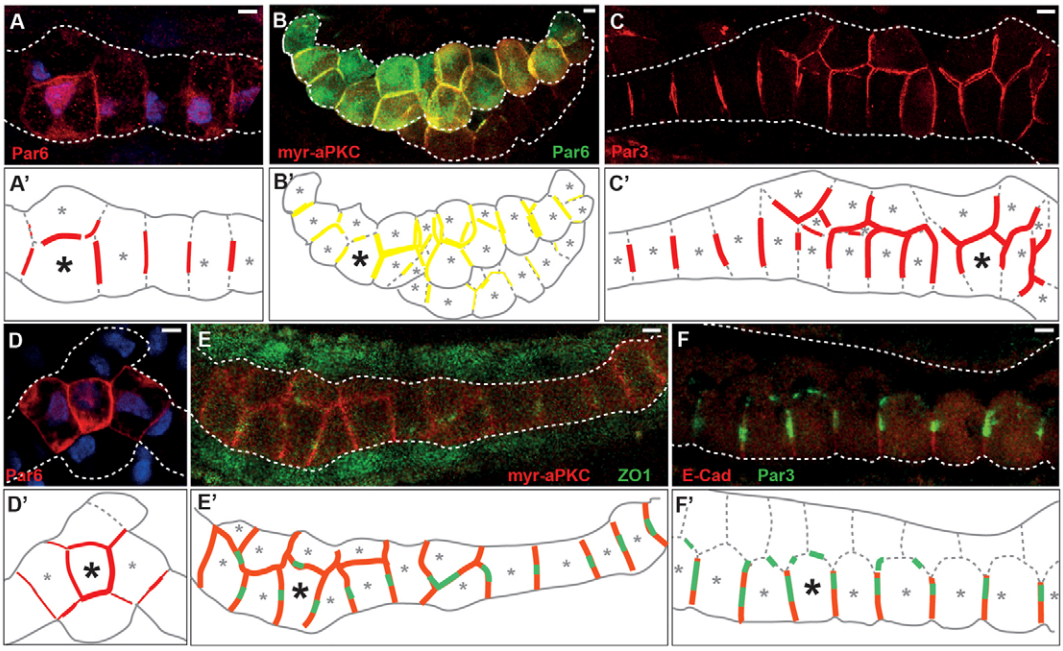


**Fig. 6. Bipolarity of notochord cells is a consequence of the tissue configuration.** (**A-F′**) Confocal images of notochord cells at stage IV expressing fluorescent fusion proteins in either wild-type embryos that had an incomplete cell intercalation (A,C,D,F, diagramed in A′,C′,D′,F′) or embryos with myr-aPKC overexpression (B,E, diagramed in B′,E′). White dashed lines indicate limits of the notochord; small asterisks mark cells positive for the transgene(s); large asterisks indicate cells displaying the characteristics described in the results. E is a section; all others are projections. Scale bars: 5 μm.

revealed Par6 was strongly expanded to the lateral and basal domains, where it co-localized with myr-aPKC (supplementary material Fig. S3E,F; Fig. 6B). By contrast, Par3 and ZO1was sharply restricted to the prospective apical domains (supplementary material Fig. S3G,H,C), and then to the apical/lateral junctions at the onset of lumen formation (supplementary material Fig. S3I,I′,D). Thus, both Par3 and ZO1 localizations were unaffected, suggesting that Par3 localization is independent of aPKC and Par6, and tight junction recruitment and localization is only Par3 dependent. Taken together, our observations suggest that the localized activity of Par3 is essential for the A-B polarization of the notochord cells, and Par3-dependent tight junction formation is a key event in lumen formation (supplementary material Fig. S4).

We also overexpressed a dominant-negative form of aPKC (kinase-dead, K197W) that has caused mislocalization of Par3 and disruption of tight junction formation in MDCK cells (Suzuki et al., 2001), but we found no disruption of Par3 localization and lumen formation (supplementary material Fig. S5A). Similarly, a dominant-negative Par6 (PAR-6 ΔaPKC-BD) lacking amino acids 1-125, which corresponds to the aPKC-binding domain (Suzuki et al., 2001), did not disrupt A-B polarization or lumen formation (supplementary material Fig. S5B). Par3 S732A, which corresponds to rat Par3 S827A that is unphosphorylatable by aPKC and has the same effect as the aPKC dominant-negative in MDCK cells (Nagai-Tamai et al., 2002), also did not disrupt the A-B polarization and lumen formation (supplementary material Fig. S5C). These observations confirm the result of myr-aPKC expression and further rule out a role for aPKC in the A-B polarization of notochord cells.

### Bipolarity of notochord cells is a consequence of the tissue configuration

An intriguing feature of *Ciona* notochord cells is their bipolarity. To obtain insights on the mechanisms responsible for its establishment, we asked whether this polarity was intrinsic to the cells, and if it could be remodeled if the cells were in a different geometrical context. To avoid modifying too many parameters, we performed this study *in vivo*, by simply observing the polarity of notochord cells in embryos that had partly failed to undergo convergent extension, either naturally or owing to myr-aPKC overexpression. When a cell possessed three neighbors (Fig. 6A), one anterior, one posterior and one medial, a third central Par6 domain appeared at the supernumerary cell-cell interface (schematized in Fig. 6A′). When a fourth cell-cell interface existed, a fourth Par6 domain appeared (Fig. 6B,B′). The same was observed with Par3 (Fig. 6C,C′). If the cell was completely surrounded by neighbors, all sides became Par6-postive (Fig. 6D,D′). The tight junction protein ZO1 also accumulated in the supernumerary Par3/6 domains (Fig. 6E,E′). Thus, the accumulation of Par3/6 and ZO1 can develop between two adjacent notochord cells, even if the cell-cell interface is not perpendicular to the A-P axis of the notochord and the embryo. In some cases, when fragment of notochord was composed of two rows of cells neatly arranged in parallel, we noticed that in the cell junctions perpendicular to the A-P axis, the Par3 domain was not in the center of the cell/cell interfaces, but was shifted towards the center of the notochord (Fig. 6F,F′). Finally, we confirmed that these new arrangements not only did not inhibit lumen formation, but the emergence of lumen pockets followed the new pattern of apical domains (supplementary material Fig. S3B,B′).

## DISCUSSION

### *Ciona* notochord cell bipolarity

Notochord cells form extracellular lumens at both sides, which are subsequently connected via cell shape changes and junction remodeling (Dong et al., 2009). Here, we demonstrate that notochord cells form two apical domains that are decorated with

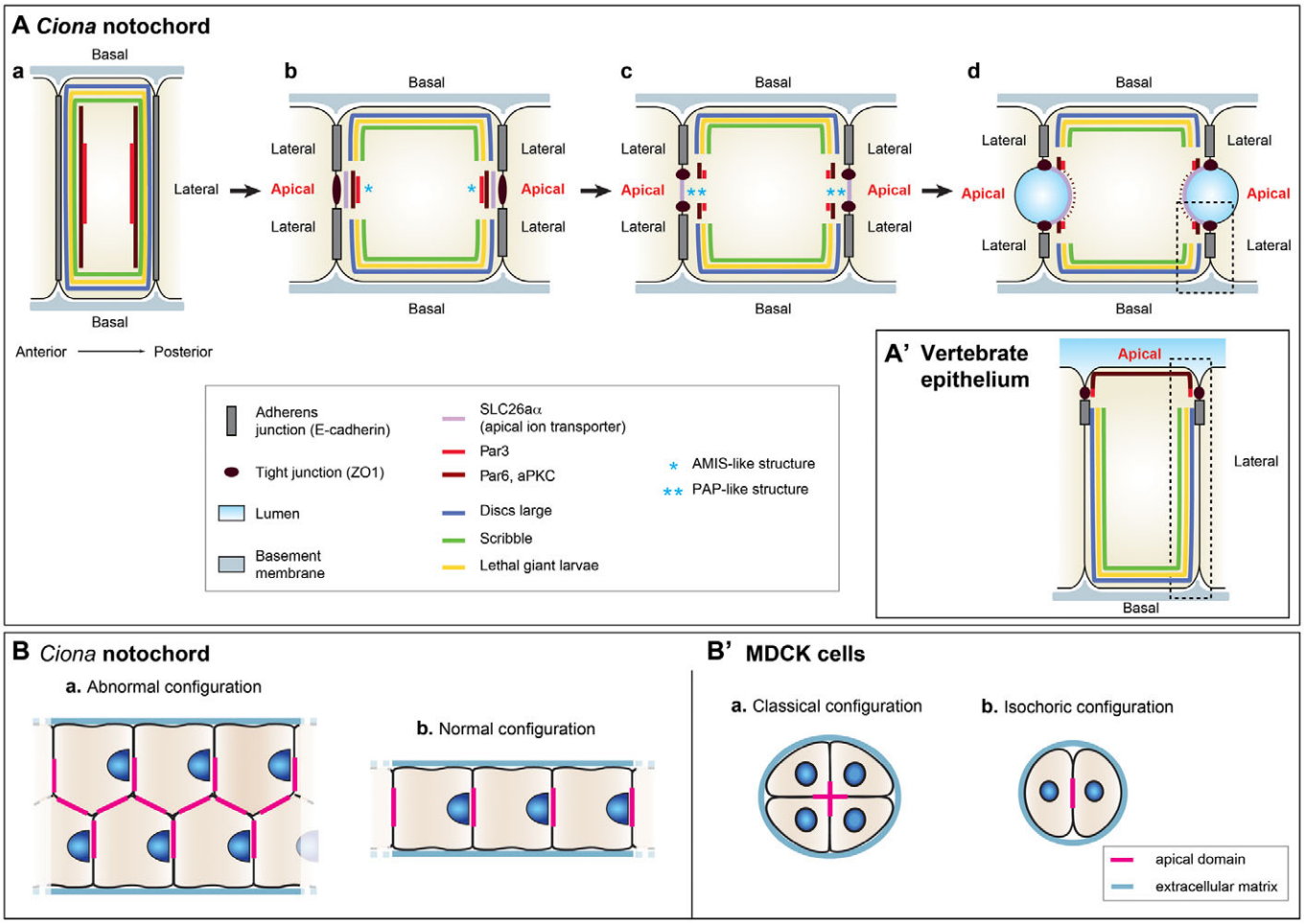


**Fig. 7. Stepwise A-B polarization of notochord cells.** (**A**,**A′**) Positions of membrane domains, cell junctions and polarity proteins in notochord cells at early stage IV (Aa), mid-stage IV (Ab), late stage IV (Ac) and stage V (Ad), and a vertebrate epithelial cell. The dashed rectangles in Ad and A′ highlight the comparable area where the spatial relationship between membrane domains, junctions and lumen is the same in both cells. (**B**,**B′**) Bipolar cells are a consequence of an atypical configuration in a classical chord-hollowing process. Comparison of the localization of the apical domain(s) in notochord cells in normal (Bb) versus abnormal (Ba) configuration with MDCK cysts in isochoric (B′b) versus classical (B′a) configuration .

specific apical markers such as the ion transporter Slc26aα and Par complex. Both domains undergo the same molecular, structural and morphological changes that occur symmetrically and often simultaneously. At a structural level, the establishment of A-B polarity in notochord cells corresponds to the symmetrical downregulation of adherens junctions between adjacent cells, and the *de novo* assembly of two sets of tight junctions per cell, at the apical-lateral boundary. Tunicates are the only metazoans other than vertebrates to possess tight junctions (Cereijido et al., 2004; Green and Bergquist, 1982; Itza and Mozingo, 2005; Lane et al., 1986; Mao et al., 1997; Spiegel and Howard, 1983). For the first time, we have followed their establishment *in vivo* at the molecular level (via ZO1), and show their importance for lumen formation in tunicates. The tight junction proteins accumulate as soon as the apical domains are specified, and as the domains mature, they are restricted to the apical/lateral interface, more apically than adherens junctions, exactly as in vertebrates (Fig. 7A,A′), and unlike what is seen in non-chordates.

It is interesting to note that at the later stage, during lumen connection, notochord cells will adopt another type of bipolarity by developing two leading edges, which crawl in opposite directions on the extracellular matrix, causing a bidirectional stretching of the cells, the retraction of the diametrically opposite cell extremities and the remodeling of cell junctions on both sides (Denker and Jiang, 2012).

## Bipolarity is generated by two individual Par3-based centers in each cell

Both apical domains of *Ciona* notochord cells are symmetrically generated and maintained by the formation of two discrete patches containing Par3, Par6 and aPKC at opposite ends of the cells (Fig. 7Aa,b). After tight junction formation, the Par proteins persistently colocalize with them (Fig. 7Ac,d), forming rings around the apical domains at the apical/lateral interfaces. The overall polarization, and the consequent formation of tight junctions and the lumen pockets are strictly dependent on Par3 activity. The key requirement for Par3 in A-B polarization during lumen formation has been implicated in other models of tubulogenesis, but often *in vitro*, and indirectly. Mice lacking Rasip1, a Ras-interacting protein, fail to form lumen in all blood vessels. Par3 in *Rasip1*$^{-/-}$ endothelial cells *in vitro* initially localizes normally to the apical domain, but is not cleared at the site when lumen formation normally occurs,

indicating a defect at the pre-lumen formation stage (Xu et al., 2011). Zovein et al. have shown that the loss of β1-integrin leads to the disruption of arterial endothelial cell polarity and lumen formation with a downregulation of Par3, and lumen formation defect can be partially rescued by the replacement of Par3 protein (Zovein et al., 2010). Notably, and paradoxically, Par3 protein localizes in this context at the basal side of endothelial cells. In this study, we directly target Par3 and show a significant disruption of the localization of other polarity proteins and structural proteins, as well as of lumen formation, indicating a central role for this polarity protein in notochord tubulogenesis (Figs 4, 5). Interestingly, as the lumen pockets enlarge over time, the tight junction ring increases its diameter without significantly changing its thickness. This implies that, not only more membrane, but also additional tight junction proteins have to be added to allow the ring to shift centrifugally in space while the lumen enlarges. The persistent spatial association of ZO1 domain and Par3 domain suggests a continuous requirement for Par3 in tight junction maintenance and restructuring (Izumi et al., 1998; Joberty et al., 2000).

### Bipolarity is a direct consequence of a more general, classical polarity establishment logic

The clear correlation between the consecutive generation of new cell-cell interfaces and the induction of ectopic apical domains at each of them demonstrates that the geometrical cell arrangement is an essential cue for the polarization process. Moreover, the apical domains emerge off-centered from their normal position and shift to the interior of the cell cluster (Fig. 7Ba). This resembles the cell polarity in multicellular cysts of MDCK cells *in vitro*, where the apical domains form in the center of the cysts, at cell-cell interfaces (Fig. 7B′a) (Datta et al., 2011). However, when MDCK cells are isolated in 'isochoric' configuration, in which only two cells undergo tubulogenesis (Fig. 7B′b) (Ferrari et al., 2008), the polarization process looks strikingly similar to what we describe at the interface of two notochord cells (Fig. 7Bb). We conclude that the bipolar feature in *Ciona* cells is a modified case of the classical chord hollowing process of MDCK cells, and is a consequence of the specific configuration of the notochord cells, i.e. a single cell-thick rod of cells. Thus, in a normal notochord, as each cylindrically shaped cell has two neighbors, each cell forms two central apical domains. Consistently, the anterior- and posterior-most notochord cells form only one apical domain because they have only one neighbor, and the other end of cell is surrounded by extracellular matrix. To generalize, we suggest that the location of the Par domains is determined in a position that is maximally distant from the extracellular matrix at the basal domain.

The molecular basis underlying this is elusive. One hypothesis is that an inhibitory signal is present that is emitted by the extracellular matrix at the basal side and forms a gradient at the cell-cell interface. The apical-forming activity, which may be an intrinsic property of the lateral domain and initially presents itself uniformly at the lateral interface, is suppressed by this inhibitory activity, except at the center, where the inhibition is lowest. Interestingly, both Par3 and Par6 initially have a broad localization at the lateral domain, before becoming enriched and restricted at the central region (Fig. 1Aa-c″). Members of integrin family receptors for extracellular matrix have recently been implicated in regulating A-B polarity in multiple systems (Datta et al., 2011; Iruela-Arispe and Davis, 2009; Myllymäki et al., 2011; O'Brien et al., 2001; Wu et al., 2009; Yu et al., 2005; Zhang et al., 2009); they may also play a role in integrating extracellular and intercellular signals to establish A-B polarity in notochord cells.

### Bipolarity as a general principle to solve geometrical constraints during tubulogenesis

The rearrangement of cells in a single file to a multicellular tube enclosing a continuous lumen presents unique challenges. It must not alter the integrity of the tissue itself nor the luminal compartment. *Ciona* notochord cells meet these challenges by becoming bipolar epithelial cells possessing two apical domains. Because the arrangement of cells in a single row before the tubulogenesis is a common configuration during development (Herwig et al., 2011; Kamei et al., 2006; Lee et al., 2003; Samakovlis et al., 1996), the presence of bipolarity is likely not unique to notochord cells. Intriguingly, Herwig et al. have recently shown that the formation of certain segments of dorsal longitudinal anastomotic vessels (DLAV) in vertebrate commences with the *de novo* establishment of lumens at both sides of the cells. The lumens between neighboring cells are connected through cell movement and cell shape changes, remarkably similar to what takes place in notochord (Herwig et al., 2011). Other cell types, including the *Drosophila* fusion cells during trachea morphogenesis and endothelial cells in vertebrate trunk intersegmental vessels during vasculogenesis involving intracellular vacuoles, also go through an transitory bipolar state, even though the tubulogenesis does not involve cord hollowing, but requires membrane fusion at the ends of the cells to create continuous lumen (Denker and Jiang, 2012). We therefore propose bipolarity, in the sense of having an axial symmetry and two apical domains at opposing ends, as a general principle to solve geometrical constraints during tubulogenesis involving a single file of cells.

### Stepwise polarization at each end of notochord cells underlying tubulogenesis

The establishment of A-B polarity at each end of notochord cells proceeds through multiple steps. Par3 and Par6, followed by aPKC, are restricted to a central spot of adherens junctions, where the future apical domain will form, before the accumulation of the apical marker Slc26aα (Fig. 7Aa). This event is similar to the accumulation of podocalyxin, the polarity proteins and the exocyst complex at a landmark named as AMIS (apical membrane initiation site) at the first stage of lumen formation in MDCK cells (Bryant et al., 2010). An interesting observation is that the accumulation of the Par complex occurs before the disruption of adherens junctions (monitored using E-Cad, Fig. 3Ca) in notochord cells, whereas the Par complex accumulates when adherens junctions have been removed (monitored with β-catenin) in MDCK cells. This suggests a potentially earlier stage, before AMIS, when the Par complex and adherens junction co-exist. The early accumulation of tight junctions (monitored by ZO1) at the center, also before the downregulation of E-Cad (Fig. 3Ea), is similar to the early presence of tight junctions in MDCK cells (monitored using occludin, although the domain is much broader than the Par complex domain), suggesting the importance of tight junctions at the early stage of lumen initiation. The specific apical transporter Slc26aα also accumulates at the site slightly later (Fig. 1B); therefore, the AMIS in notochord cells transiently contains Par3, Par6, aPKC, ZO1, E-Cad and Slc26aα (Fig. 7Ab). Still before any lumen can be observed, Par3, Par6, aPKC and ZO1 become excluded from the apical domain, which Slc26aα occupies exclusively, and form the apical/lateral border (Fig. 7Ac). Concomitantly, the apical domain is cleared of adherens junction proteins and of basolateral markers Lgl, Scribble and Dlg. This spatial organization parallels the maturation of the AMIS into a PAP (pre-apical patch) in MDCK cells, where the Par complex resolves from apical marker

podocalyxin, and localizes to the newly consolidated tight junctions around the apical domain, before lumen starts to appear (Bryant et al., 2010). Structures similar to AMIS and PAP have been reported in other contexts, including in mouse aorta lumenogenesis (containing F-actin, myosin, ERM and CD34) (Strilić et al., 2009), during the formation of the 'intracellular' lumen of *Drosophila* terminal tracheal cells (containing Par complex, crumbs complex, F-actin and microtubules) (Gervais and Casanova, 2010), and at the apical domain of zebrafish neuroepithelium presaging lumen formation (Par3) (Tawk et al., 2007). These and our observations support a common *de novo* and progressive lumen-initiating mechanism both in 3D culture and *in vivo* (Datta et al., 2011). During the subsequent lumen formation phase, comparable with the open lumen stage in MDCK cells, polarity proteins continue to localize specifically at the apical/lateral boundary of notochord cells, suggesting an involvement in the maintenance of cell polarity (Fig. 7Ad).

## Relative functions of Par3, Par6 and aPKC

In *Ciona* notochord, Par3 knockdown affects both Par6 and aPKC localization, indicating that aPKC and Par6 localizations are Par3 dependent. Mislocalization of aPKC (myr-aPKC) at the basal and lateral domains causes a broader Par6 distribution but leaves Par3 unaffected, suggesting Par6 localization is aPKC dependent but Par3 localization is not. Moreover, ZO1 is correctly positioned in the myr-aPKC cells, and lumen is able to form, whereas Par3 depletion causes an abnormal recruitment of ZO1, mislocalization of tight junctions and blocks lumen formation. These results are congruent in concluding that Par3 is the key molecule in A-B polarization of notochord cells. Its restricted subcellular localization, but not that of Par6 and aPKC, is crucial for the formation of the apical domain, the positioning of tight junctions and lumen formation. These data confirm an increasing number of studies reporting the independence between Par3 and aPKC. For example, in MDCK cells, Par3 can control tight junction assembly through its Par6/aPKC-independent interaction with Tiam1 (Chen and Macara, 2005), and in endothelial cells in culture, Par3 can associate with VE-cadherin in the absence of aPKC and prior to the association of Par6 (Iden et al., 2006). In *Drosophila* embryonic epithelial cells, as in *Ciona* notochord, the localization of Par3 homologue (Bazooka) is independent of aPKC, but aPKC (and Par6) localization is Par3 dependent (Harris and Peifer, 2005). All these studies and this report bring a new vision of Par3 in the context of epithelial cells, as a protein that is specifically responsible for junction positioning, working independently or sometimes antagonistically of aPKC (Chen and Macara, 2005; Ferrari et al., 2008; St Johnston and Sanson, 2011).

## Co-option of a polarity mechanism is associated with an innovative strategy to make the notochord a hydrostatic skeleton

The last interesting perspective concerns the evolution of notochord and the strategies used to make it a stiff yet flexible rod, acting as a hydrostatic skeleton to aid swimming. Two strategies exist within chordates. In vertebrates and cephalochordates, notochord cells develop large fluid-filled vacuoles that remain intracellular, whereas in urochordates, the notochord undergoes tubulogenesis and lumens are extracellular. The current chordate phylogeny (Delsuc et al., 2008) positions the urochordates as a sister group of vertebrates, suggesting that the ancestral state is the presence of vacuoles, in non-A-B polarized cells. Consequently, the presence of A-B polarity in the notochord cells of urochordates is a derived feature, suggesting that in this lineage there was a co-option of a universal polarization mechanism to generate the notochord tube, allowing a new strategy for tail extension and tadpole-like swimming behavior. It will be interesting to investigate the mechanistic link between vacuole formation and lumen formation that can explain these evolutionary diversities.

**Acknowledgements**
We thank Andreas Wodarz for providing anti-Bazooka/Par3 antibody; François Robin for providing ZO1 and Lgl entry clones; Bradley Davidson for providing myr-aPKC plasmid; Janet Chenevert, Agnès Roure and Patrick Lemaire for providing gateway-compatible cDNA clones; and William Smith for hosting Elsa Denker at UCSB. We thank Mary Laplante, Gemma Richards, Eric Thompson and Daniel Chourrout for critical reading of the manuscript.

**Funding**
This work was supported by the Norwegian Research Council [133335/V40 and 183302/S10 to D.J.].

**Competing interests statement**
The authors declare no competing financial interests.

**Author contributions**
E.D. and D.J. conceived the project and contributed equally to the manuscript. I.B. performed the transmission electron microscopy. All other experimental data were generated by E.D. D.J. designed the FPapkc primers.

**Supplementary material**
Supplementary material available online at
http://dev.biologists.org/lookup/suppl/doi:10.1242/dev.092387/-/DC1

**References**

**Baer, M. M., Chanut-Delalande, H. and Affolter, M.** (2009). Cellular and molecular mechanisms underlying the formation of biological tubes. *Curr. Top. Dev. Biol.* **89**, 137-162.
**Bryant, D. M. and Mostov, K. E.** (2008). From cells to organs: building polarized tissue. *Nat. Rev. Mol. Cell Biol.* **9**, 887-901.
**Bryant, D. M., Datta, A., Rodríguez-Fraticelli, A. E., Peränen, J., Martín-Belmonte, F. and Mostov, K. E.** (2010). A molecular network for de novo generation of the apical surface and lumen. *Nat. Cell Biol.* **12**, 1035-1045.
**Cereijido, M., Contreras, R. G. and Shoshani, L.** (2004). Cell adhesion, polarity, and epithelia in the dawn of metazoans. *Physiol. Rev.* **84**, 1229-1262.
**Chen, X. and Macara, I. G.** (2005). Par-3 controls tight junction assembly through the Rac exchange factor Tiam1. *Nat. Cell Biol.* **7**, 262-269.
**Christiaen, L., Wagner, E., Shi, W. and Levine, M.** (2009). Microinjection of morpholino oligos and RNAs in sea squirt (Ciona) embryos. *Cold Spring Harb. Protoc.* **2009**, t5347.
**Datta, A., Bryant, D. M. and Mostov, K. E.** (2011). Molecular regulation of lumen morphogenesis. *Curr. Biol.* **21**, R126-R136.
**Delsuc, F., Tsagkogeorga, G., Lartillot, N. and Philippe, H.** (2008). Additional molecular support for the new chordate phylogeny. *Genesis* **46**, 592-604.
**Denker, E. and Jiang, D.** (2012). Ciona intestinalis notochord as a new model to investigate the cellular and molecular mechanisms of tubulogenesis. *Semin. Cell Dev. Biol.* **23**, 308-319.
**Dong, B., Horie, T., Denker, E., Kusakabe, T., Tsuda, M., Smith, W. C. and Jiang, D.** (2009). Tube formation by complex cellular processes in Ciona intestinalis notochord. *Dev. Biol.* **330**, 237-249.
**Ferrari, A., Veligodskiy, A., Berge, U., Lucas, M. S. and Kroschewski, R.** (2008). ROCK-mediated contractility, tight junctions and channels contribute to the conversion of a preapical patch into apical surface during isochoric lumen initiation. *J. Cell Sci.* **121**, 3649-3663.
**Gervais, L. and Casanova, J.** (2010). In vivo coupling of cell elongation and lumen formation in a single cell. *Curr. Biol.* **20**, 359-366.
**Green, C. R. and Bergquist, P. R.** (1982). Phylogenetic relationships within the invertebrata in relation to the structure of septate junctions and the development of 'occluding' junctional types. *J. Cell Sci.* **53**, 279-305.
**Harris, T. J. and Peifer, M.** (2005). The positioning and segregation of apical cues during epithelial polarity establishment in Drosophila. *J. Cell Biol.* **170**, 813-823.
**Herwig, L., Blum, Y., Krudewig, A., Ellertsdottir, E., Lenard, A., Belting, H. G. and Affolter, M.** (2011). Distinct cellular mechanisms of blood vessel fusion in the zebrafish embryo. *Curr. Biol.* **21**, 1942-1948.
**Iden, S., Rehder, D., August, B., Suzuki, A., Wolburg-Buchholz, K., Wolburg, H., Ohno, S., Behrens, J., Vestweber, D. and Ebnet, K.** (2006). A distinct PAR complex associates physically with VE-cadherin in vertebrate endothelial cells. *EMBO Rep.* **7**, 1239-1246.
**Iruela-Arispe, M. L. and Davis, G. E.** (2009). Cellular and molecular mechanisms of vascular lumen formation. *Dev. Cell* **16**, 222-231.

**Itza, E. M. and Mozingo, N. M.** (2005). Septate junctions mediate the barrier to paracellular permeability in sea urchin embryos. *Zygote* **13**, 255-264.
**Izumi, Y., Hirose, T., Tamai, Y., Hirai, S., Nagashima, Y., Fujimoto, T., Tabuse, Y., Kemphues, K. J. and Ohno, S.** (1998). An atypical PKC directly associates and colocalizes at the epithelial tight junction with ASIP, a mammalian homologue of Caenorhabditis elegans polarity protein PAR-3. *J. Cell Biol.* **143**, 95-106.
**Jiang, D. and Smith, W. C.** (2007). Ascidian notochord morphogenesis. *Dev. Dyn.* **236**, 1748-1757.
**Joberty, G., Petersen, C., Gao, L. and Macara, I. G.** (2000). The cell-polarity protein Par6 links Par3 and atypical protein kinase C to Cdc42. *Nat. Cell Biol.* **2**, 531-539.
**Kamei, M., Saunders, W. B., Bayless, K. J., Dye, L., Davis, G. E. and Weinstein, B. M.** (2006). Endothelial tubes assemble from intracellular vacuoles in vivo. *Nature* **442**, 453-456.
**Lane, N. J., Dallai, R., Burighel, P. and Martinucci, G. B.** (1986). Tight and gap junctions in the intestinal tract of tunicates (Urochordata): a freeze-fracture study. *J. Cell Sci.* **84**, 1-17.
**Lee, M., Lee, S., Zadeh, A. D. and Kolodziej, P. A.** (2003). Distinct sites in E-cadherin regulate different steps in Drosophila tracheal tube fusion. *Development* **130**, 5989-5999.
**Lubarsky, B. and Krasnow, M. A.** (2003). Tube morphogenesis: making and shaping biological tubes. *Cell* **112**, 19-28.
**Macara, I. G.** (2004). Parsing the polarity code. *Nat. Rev. Mol. Cell Biol.* **5**, 220-231.
**Mao, B., Sun, X., Zhang, H., Zhang, S. and Wu, X.** (1997). Morphological and functional studies on the epidermal cells of amphioxus (Branchiostoma belcheri tsingtauense) at different developmental stages. *Chin. J. Oceanology Limnol.* **15**, 236-241.
**McCaffrey, L. M. and Macara, I. G.** (2009). Widely conserved signaling pathways in the establishment of cell polarity. *Cold Spring Harb. Perspect. Biol.* **1**, a001370.
**Myllymäki, S. M., Teräväinen, T. P. and Manninen, A.** (2011). Two distinct integrin-mediated mechanisms contribute to apical lumen formation in epithelial cells. *PLoS ONE* **6**, e19453.
**Nagai-Tamai, Y., Mizuno, K., Hirose, T., Suzuki, A. and Ohno, S.** (2002). Regulated protein-protein interaction between aPKC and PAR-3 plays an essential role in the polarization of epithelial cells. *Genes Cells* **7**, 1161-1171.
**O'Brien, L. E., Jou, T. S., Pollack, A. L., Zhang, Q., Hansen, S. H., Yurchenco, P. and Mostov, K. E.** (2001). Rac1 orientates epithelial apical polarity through effects on basolateral laminin assembly. *Nat. Cell Biol.* **3**, 831-838.
**Patalano, S., Prulière, G., Prodon, F., Paix, A., Dru, P., Sardet, C. and Chenevert, J.** (2006). The aPKC-PAR-6-PAR-3 cell polarity complex localizes to the centrosome attracting body, a macroscopic cortical structure responsible for asymmetric divisions in the early ascidian embryo. *J. Cell Sci.* **119**, 1592-1603.
**Roure, A., Rothbächer, U., Robin, F., Kalmar, E., Ferone, G., Lamy, C., Missero, C., Mueller, F. and Lemaire, P.** (2007). A multicassette Gateway vector set for high throughput and comparative analyses in ciona and vertebrate embryos. *PLoS ONE* **2**, e916.
**Samakovlis, C., Manning, G., Steneberg, P., Hacohen, N., Cantera, R. and Krasnow, M. A.** (1996). Genetic control of epithelial tube fusion during Drosophila tracheal development. *Development* **122**, 3531-3536.
**Sherrard, K., Robin, F., Lemaire, P. and Munro, E.** (2010). Sequential activation of apical and basolateral contractility drives ascidian endoderm invagination. *Curr. Biol.* **20**, 1499-1510.
**Spiegel, E. and Howard, L.** (1983). Development of cell junctions in sea-urchin embryos. *J. Cell Sci.* **62**, 27-48.
**St Johnston, D. and Sanson, B.** (2011). Epithelial polarity and morphogenesis. *Curr. Opin. Cell Biol.* **23**, 540-546.
**Strilić, B., Kucera, T., Eglinger, J., Hughes, M. R., McNagny, K. M., Tsukita, S., Dejana, E., Ferrara, N. and Lammert, E.** (2009). The molecular basis of vascular lumen formation in the developing mouse aorta. *Dev. Cell* **17**, 505-515.
**Suzuki, A. and Ohno, S.** (2006). The PAR-aPKC system: lessons in polarity. *J. Cell Sci.* **119**, 979-987.
**Suzuki, A., Yamanaka, T., Hirose, T., Manabe, N., Mizuno, K., Shimizu, M., Akimoto, K., Izumi, Y., Ohnishi, T. and Ohno, S.** (2001). Atypical protein kinase C is involved in the evolutionarily conserved par protein complex and plays a critical role in establishing epithelia-specific junctional structures. *J. Cell Biol.* **152**, 1183-1196.
**Tawk, M., Araya, C., Lyons, D. A., Reugels, A. M., Girdler, G. C., Bayley, P. R., Hyde, D. R., Tada, M. and Clarke, J. D.** (2007). A mirror-symmetric cell division that orchestrates neuroepithelial morphogenesis. *Nature* **446**, 797-800.
**Wada, S., Katsuyama, Y., Yasugi, S. and Saiga, H.** (1995). Spatially and temporally regulated expression of the LIM class homeobox gene Hrlim suggests multiple distinct functions in development of the ascidian, Halocynthia roretzi. *Mech. Dev.* **51**, 115-126.
**Wei, X., Cheng, Y., Luo, Y., Shi, X., Nelson, S. and Hyde, D. R.** (2004). The zebrafish Pard3 ortholog is required for separation of the eye fields and retinal lamination. *Dev. Biol.* **269**, 286-301.
**Wodarz, A., Ramrath, A., Kuchinke, U. and Knust, E.** (1999). Bazooka provides an apical cue for Inscuteable localization in Drosophila neuroblasts. *Nature* **402**, 544-547.
**Wu, W., Kitamura, S., Truong, D. M., Rieg, T., Vallon, V., Sakurai, H., Bush, K. T., Vera, D. R., Ross, R. S. and Nigam, S. K.** (2009). Beta1-integrin is required for kidney collecting duct morphogenesis and maintenance of renal function. *Am. J. Physiol.* **297**, F210-F217.
**Xu, K., Sacharidou, A., Fu, S., Chong, D. C., Skaug, B., Chen, Z. J., Davis, G. E. and Cleaver, O.** (2011). Blood vessel tubulogenesis requires Rasip1 regulation of GTPase signaling. *Dev. Cell* **20**, 526-539.
**Yu, W., Datta, A., Leroy, P., O'Brien, L. E., Mak, G., Jou, T. S., Matlin, K. S., Mostov, K. E. and Zegers, M. M.** (2005). Beta1-integrin orients epithelial polarity via Rac1 and laminin. *Mol. Biol. Cell* **16**, 433-445.
**Zhang, X., Mernaugh, G., Yang, D. H., Gewin, L., Srichai, M. B., Harris, R. C., Iturregui, J. M., Nelson, R. D., Kohan, D. E., Abrahamson, D. et al.** (2009). beta1 integrin is necessary for ureteric bud branching morphogenesis and maintenance of collecting duct structural integrity. *Development* **136**, 3357-3366.
**Zovein, A. C., Luque, A., Turlo, K. A., Hofmann, J. J., Yee, K. M., Becker, M. S., Fassler, R., Mellman, I., Lane, T. F. and Iruela-Arispe, M. L.** (2010). Beta1 integrin establishes endothelial cell polarity and arteriolar lumen formation via a Par3-dependent mechanism. *Dev. Cell* **18**, 39-51.

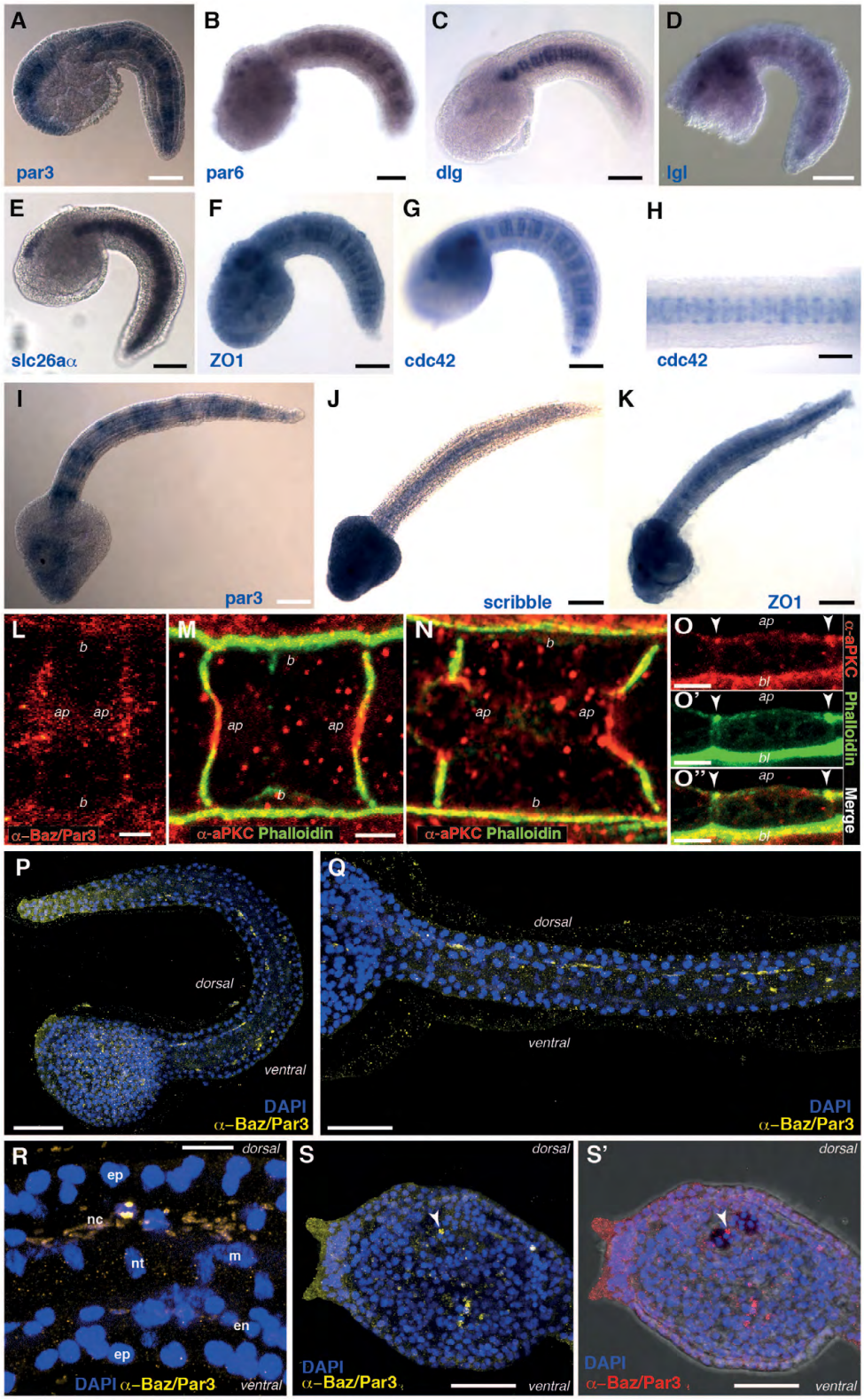


**Fig. S1. Expression profiles of the candidate genes investigated in this study.** (**A-G**) At early stage IV, *par3* (A), *par6* (B), *dlg* (C), *lgl* (D), *slc26aα* (E), *zo1* (F) and *cdc42* (G) transcripts are strongly expressed in the notochord and in groups of cells in the head, which are likely associated with developing neural structures. (**H-K**) At late stage IV, *par3* (I), *scribble* (J), *zo1* (K) and *cdc42* (H) are still strongly expressed in the notochord and in the head. *par3* also appears in scattered groups of cells dorsal to the notochord in the tail. (**L-N**) At the protein level, Par3 (L) and aPKC (M) are accumulated at the prospective apical domain of the notochord cells. When lumen opens, aPKC is restricted to the lateral/luminal boundaries (N). (**O-O″**) aPKC is also found at the lateral/apical boundaries in epidermal cells (white arrowheads). (**P-R**) In addition, Par3 is present in dorsal groups of cells that correspond to the developing nervous system in the tail. (**S**,**S′**) In the head, several groups of cells are stained, including cells in the developing sensory vesicles (white arrowhead). (L) Early stage IV; (M,P,Q) late stage IV/stage V; (N,R-S′) stage V. Scale bars: 50 µm in A-G,I-K,P,Q,S; 25 µm in H; 7 µm in L, 4 µm in M-O″; 12 µm in R. ap, apical; bl, basolateral; b, basal; ep, epidermis; nc, nerve cord; nt, notochord; m, muscle; en, endoderm.

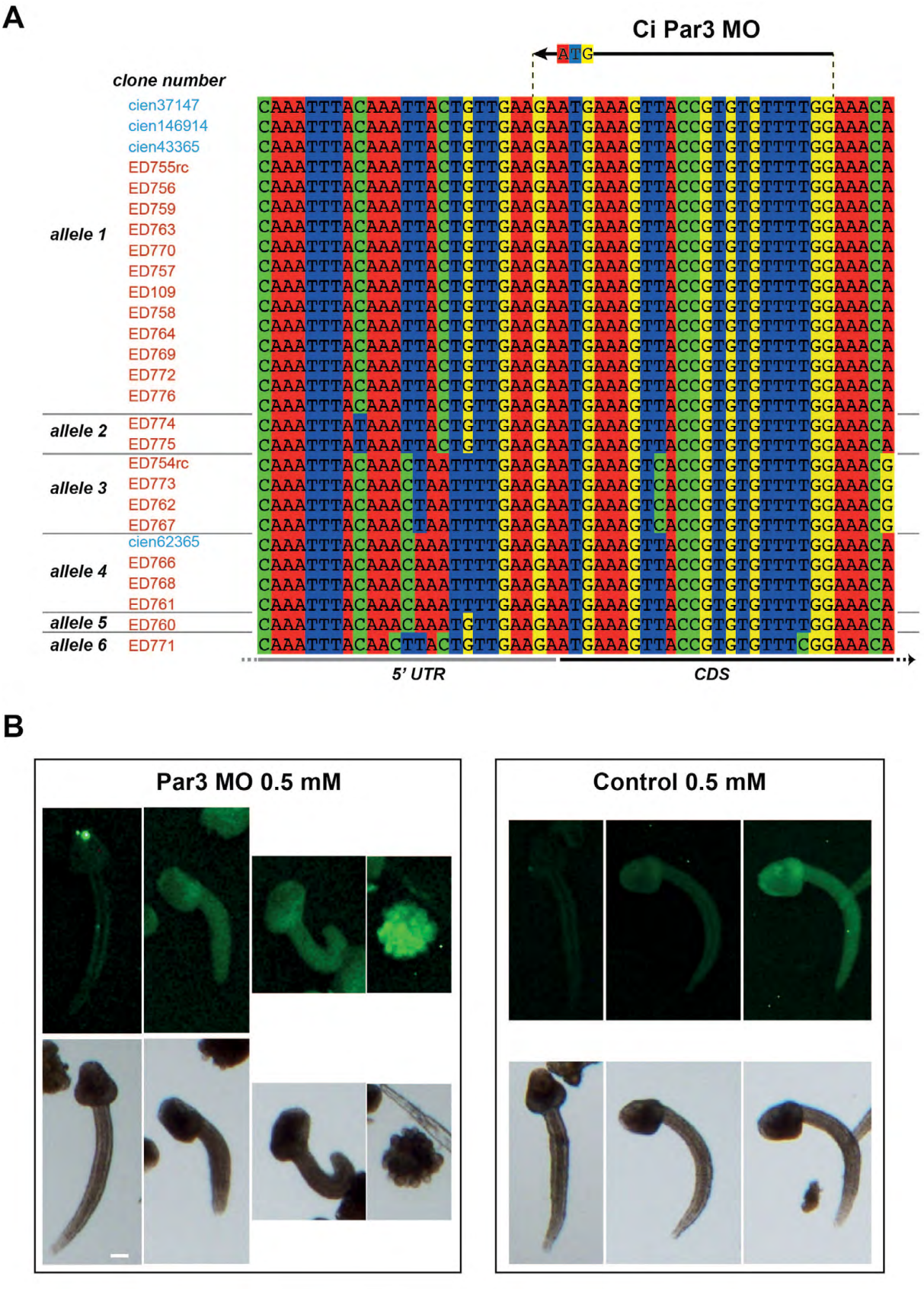


**Fig. S2. Par3 morpholino design and injection.** (**A**) Alignment of *Ciona par3* sequences from EST clones (blue, from Roscoff animals) and cDNA clones (red, Norwegian animals), showing the polymorphism and the position of the translation-blocking MO with respect to the coding sequence (CDS) and the 5′ untranslated region (5′UTR). (**B**) Dose-dependent effect of the MO on development. Increasing the amount of Par3 MO injected, which is visualized as more intense fluorescence in the embryo (left), results in more severe phenotype. This is not the case for the control MO (right). Scale bar: 50 μm.

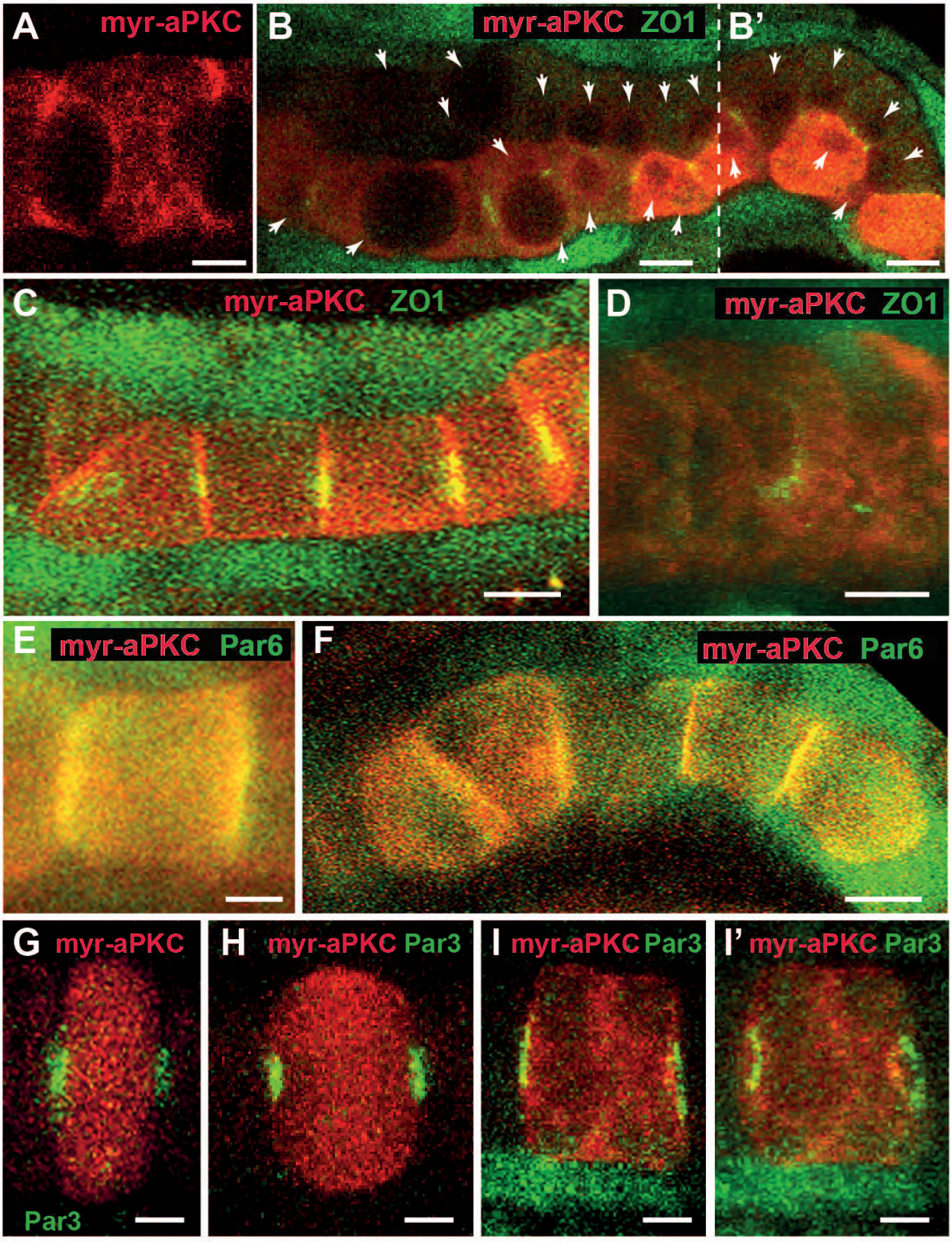


**Fig. S3. Effects of the myr-apkc overexpression.** (**A-B′**) Lumen forms after myr-apkc overexpression (A), and even with cell intercalation defects (B,B′). Arrowheads indicate lumen pockets. (**C-I′**) Subcellular localization of polarity and junction markers after myr-apkc overexpression. Par6 is mislocalized (E,F), whereas Par3 (G-I′) and ZO1 (C,D) are localized normally. All images are maximum projections except A-B′, which are sections. B and B′ are two different regions of same notochord, to show as many lumen pockets as possible. The cells in D have been rotated to show the lateral surface. I′ is the same cell in I but slightly rotated to show the Par3 rings. (A-B′) Stage V; (C,E,F,H) mid stage IV; (D,I,I′) late stage IV/stage V; (G) early stage IV. Scale bars: 5 μm in A,B,B′,D,E,G-I′; 10 μm in C,F.

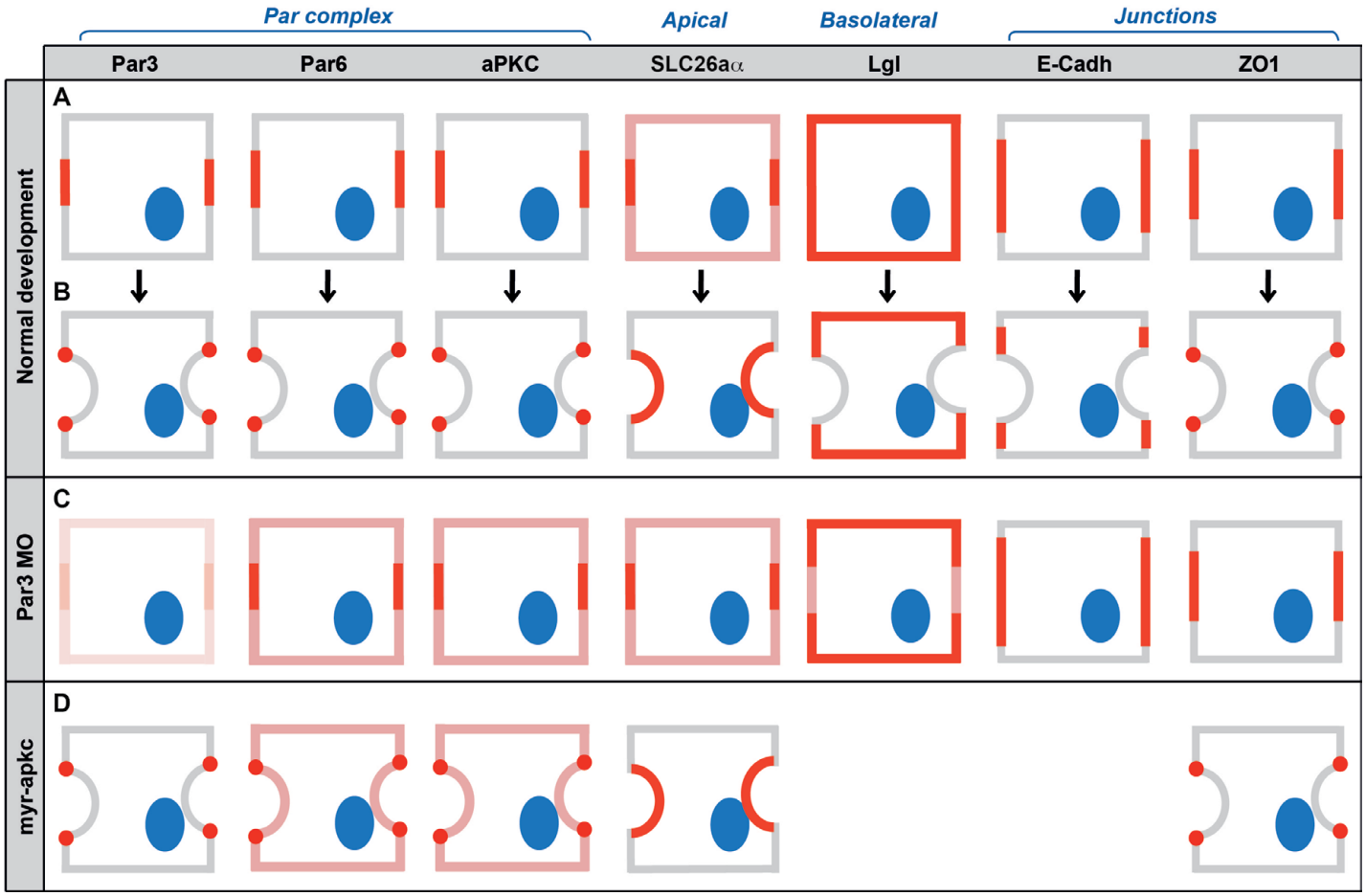


**Fig. S4. Recapitulative diagrams to compare results from myr-apkc overexpression (Fig. S3) and Par3 MO (Fig. 5).** Comparison of the localization of markers from stage IV (**A**) to stage V (**B**) during normal development to the localization of markers in Par3 morphant (**C**) and in myr-apkc overexpressing embryos (**D**) at stage V.

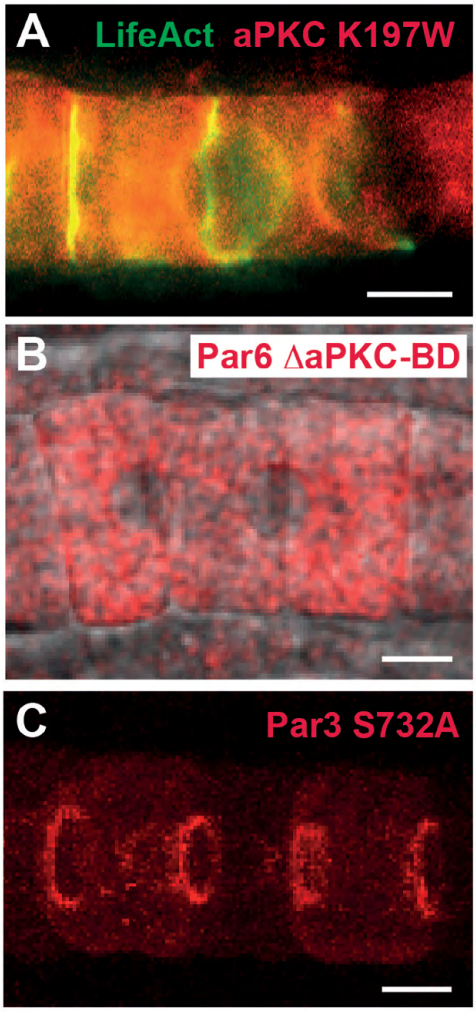


**Fig. S5. Effects of the overexpression of dominant-negative Par3, Par6 and aPKC.** (**A**) aPKC K197W mutant. (**B**) Par6 ΔaPKC-BD mutant. (**C**) Par3 S732A mutant. At stage V, the mutant-expressing cells form lumen pockets, suggesting that these mutants do not disrupt cell polarization, junction development and lumen formation. Scale bars: 10 μm.


**Movie 1. Subcellular localization of Par3 and Par6 during notochord tubulogenesis.** Time-lapse movie of notochord cells expressing turboGFP-Par6 (green) and mCherry-Par3 (red). Frame interval: 10 minutes.


**Movie 2. Subcellular localization of Par6 and Slc26aα during notochord tubulogenesis.** Time-lapse movie of notochord cells expressing turboGFP-Par6 (green) and Slc26aα-mCherry (red). Frame interval: 10 minutes.


**Movie 3. Relative subcellular localizations of Par3 and ZO1 during notochord tubulogenesis.** Time-lapse movie of notochord cells expressing ZO1-turboGFP (green) and mCherry-Par3 (red). Frame interval: 10 minutes.

**Table S1. Generation of entry clones for probe synthesis and construction of fluorescent fusion proteins**

| Gene | Transcript model | Release1 gene collection clone for probe synthesis | Gilchrist library full-length clone for entry clone | Primers to generate entry clone | | Fusion type |
|---|---|---|---|---|---|---|
| ***par3*** | KH.L147.28.v1.A.SL1-1 | R1CiGC03j17 | cien37147 | Par3-5 (ATGAAAGTTACCGTGTGTTTTGG) | Par3-3 (TTACAGATTATACGGAACAG) | N |
| ***par3 (S732A mutant)*** | | – | template: par3 entry clone above | Par3 S732A-5 (CCGCGAATCTGTCACTCGTCAAGCAATGTCGGAGAAACG) | Par3 S732A-3 (CGTTTCTCCGACATTGCTTGACGAGTGACAGATTCGCGG) | N |
| ***par6*** | KH.C6.278.v1.A.SL1-1 | – | cien151332 | Par6-5 (ATGGATAAGTTATCATTGGG) | Par6-3 (TTATATTGAAACATTAGGG) | N |
| ***par6 (ΔapKC-BD mutant)*** | | – | template: par6 entry clone above | Par6DapBD-5 (GGTACCATGATTAGTTTTCCGGAAG) | Par6DapBD-3 (TTATATTGAAACATTAGGGTTACTGC) | N |
| ***apkc*** | KH.C14.47.v1.A.SL1-1 | – | cien228658 | FPaPKC-5 (ATGTCCATAGACGCTGGTTCA) | FPaPKC-3 (TCACACAGCAACATCACTCGT) | N |
| ***apkc (K197W mutant)*** | | – | template: apkc entry clone above | aPKCK197W-5 (CGGACAAAATGTATGCTATGTGGGTAATAAAGAAAGAGTTAGT) | aPKCK197W-3 (ACTAACTCTTTCTTTATTACCCACATAGCATACATTTTGTCCG) | N |
| ***dlg*** | KH.C1.637.v1.A.ND4-1 | R1CiGC19e17 | cien185023 | dlg-5 (CAGAAAAAATGCCTGTGAGAAAACAAGATGC) | dlg-3 (TAAGTCATCAGATGCAGGCACCCATAC) | C |
| ***scribble*** | KH.C2.370.v1.A.SL1-1 | R1CiGC44l23 | cien155708 | scribble-5 (ATGTCTCCAGCAAGATTATGG) | scribble-3 (CTAGGTCATCGCTGGCTGTTG) | N |
| ***myr-apkc*** | – | – | – | CfusMyr-aPKC5 (CAGACAAAATGGGGAGCAGCAAGAGC) | CfusCMyr-aPKC3 (CACGGACTCCTCAGCAGACAGC) | C |

References for the transcript models, the clones used for probe synthesis, and the clones and primers used to generate N- or C-tagged fusion constructs.